Observations of "Hysteresis" in Backscattered Ultraviolet Ozone Data

MATTHEW T. DELAND, RICHARD P. CEBULA, LIANG-KANG HUANG, AND STEVEN L. TAYLOR

Raytheon ITSS Corporation, Lanham, Maryland

RICHARD S. STOLARSKI AND RICHARD D. MCPETERS

NASA Goddard Space Flight Center, Greenbelt, Maryland

(Manuscript received 7 March 2000, in final form 14 September 2000)

ABSTRACT

Satellite measurements using the backscattered ultraviolet technique provide a powerful method for the observation of stratospheric ozone. However, rapid input signal variations over three to four orders of magnitude in several minutes can lead to problems with instrument response. Inflight data have recently been used to characterize a "hysteresis" problem on the *NOAA-9* SBUV/2 instrument, which affects measurements made shortly after emerging from darkness. Radiance values observed under these conditions can be up to 2%–3% lower than expected. A correction has been derived for *NOAA-9* data that is solar zenith angle dependent and varies in amplitude and time. Typical changes to affected polar total ozone values are on the order of 1% but can reach 5% in some cases. Profile ozone changes are altitude dependent, with maximum values of 4%–5% at 1 hPa. The *NOAA-11* and *NOAA-14* SBUV/2 instruments have a much smaller hysteresis effect than that observed for *NOAA-9* SBUV/2 due to a change in photomultiplier tubes. The *Nimbus-7* SBUV instrument also shows a hysteresis effect, which has not been fully characterized at this time.

1. Introduction

The measurement of stratospheric ozone from space using the backscattered ultraviolet (buv) technique was first proposed by Singer and Wentworth (1957). Since that time, the National Aeronautics and Space Administration (NASA) and National Oceanic and Atmospheric Administration (NOAA) have flown multiple instruments using this technique, beginning with *Nimbus-4* BUV (Heath et al. 1973; Stolarski et al. 1997), continuing with *Nimbus-7* SBUV (Heath et al. 1975; Bhartia et al. 1995), and culminating in the SBUV/2 (solar backscatter ultraviolet, model 2) series of instruments on *NOAA-9* (Frederick et al. 1986; Ahmad et al. 1994; Lienesch et al. 1996), *NOAA-11* (Planet et al. 1994; Hilsenrath et al. 1995a), and *NOAA-14* (Hilsenrath et al. 1995b). While there are slight differences between these individual instruments, the basic measurement technique has remained unchanged. Measurements of backscattered UV radiance $I(\lambda)$ at 12 discrete wavelengths between approximately 250–340 nm are made almost continuously on the sunlit side of the spacecraft orbit. Regular measurements of solar irradiance $F(\lambda)$ are also made at the same 12 wavelengths so that albedo values (defined as $\alpha = IF^{-1}$) are constructed for each scan. These albedo values are then inverted through a radiative transfer model to extract the stratospheric ozone profile and total column ozone abundance for the scan. In this paper, we discuss a specific aspect of the SBUV/2 radiance measurements, which can lead to ozone errors immediately after the spacecraft emerges from darkness, when signal levels increase by four orders of magnitude in a few minutes. These errors can reach 5% in upper stratospheric profile ozone for the *NOAA-9* SBUV/2 instrument. The error is caused by the sensitivity of the photomultiplier tube (PMT) gain to preconditioning parameters such as signal strength and exposure time. This effect, known as hysteresis, varies in behavior between different PMTs, even from the same manufacturer. Section 2 discusses the SBUV/2 instrument and the details of the measurement sequence that lead to the existence of a hysteresis effect. Section 3 presents examples of hysteresis in *NOAA-9* SBUV/2 data and demonstrates variability in both solar zenith angle and time. Section 4 describes our operational correction for the *NOAA-9* data and discusses the impact on total ozone and profile ozone products. Section 5 discusses evidence for hysteresis in other SBUV/2 instruments, and section 6 presents our conclusions.

Corresponding author address: Matthew DeLand, Science Systems and Applications, Inc., 10210 Greenbelt Rd., Suite 400, Lanham, MD 20706.
E-mail: matt_deland@sesda.com

2. SBUV/2 instrument design and measurements

The SBUV/2 instrument design and operations are described by Frederick et al. (1986). Briefly, the SBUV/

TABLE 1. Nominal SBUV/2 wavelengths.

Channel	Wavelength (nm)
1	252.0
2	273.5
3	283.1
4	287.6
5	292.3
6	297.5
7	301.9
8	305.8
9	312.5
10	317.5
11	331.2
12	339.8

2 instrument is a nadir-viewing Ebert–Fastie double monochromator with a bandpass of 1.1 nm. It has a field of view of 11.3° × 11.3°, corresponding to a surface footprint of approximately 170 km × 170 km. The standard operating mode for an SBUV/2 instrument is to make repeated 32-s scans through 12 selected wavelengths between 252 and 340 nm. The nominal SBUV/2 wavelengths are listed in Table 1. During a single scan, each wavelength is sequentially sampled for 2 s (0.75 s for the grating drive to step to the selected position and lock, 1.25 s for signal integration) beginning at the shortest wavelength, followed by an 8-s period to return the grating drive to the starting position and collect calibration data. Figure 1 shows a typical SBUV/2 radiance spectrum for a solar zenith angle (SZA) of 40°. The nominal SBUV/2 wavelengths listed in Table 1 are identified by vertical lines. The observed radiance increases by four orders of magnitude during a single scan. Variations in surface reflectivity and SZA increase the overall range of radiance values by an additional factor of 20–50.

Three electronic gain ranges are used to accommodate the wide range of input signal strength experienced during these measurements, with range 1 being the most sensitive and ranges 2 and 3 less sensitive by successive factors of about 100. The range 1 and 2 signals are read from the last dynode of the PMT with the range 1 readout passing through an additional electronic amplification of approximately 100. The range 3 signal is read directly from the photocathode of the PMT. While the gain of the PMT for range 2 signal is approximately 500, the range 3 cathode signal is amplified by a factor of 5 prior to reaching the counter. This produces the approximate factor of 100 difference between range 2 and range 3 sensitivity. All three signals are read out simultaneously for each sample with 16-bit digitization, giving a maximum value of 65 535 counts.

Under typical midlatitude afternoon viewing conditions, the longest four wavelengths have valid signals in range 3, the middle four wavelengths are valid in range 2, and the shortest four wavelengths are valid in range 1. For measurements at high solar zenith angles, the signal level (and thus average PMT current) is reduced by a factor of 10–20, leading to a different dis-

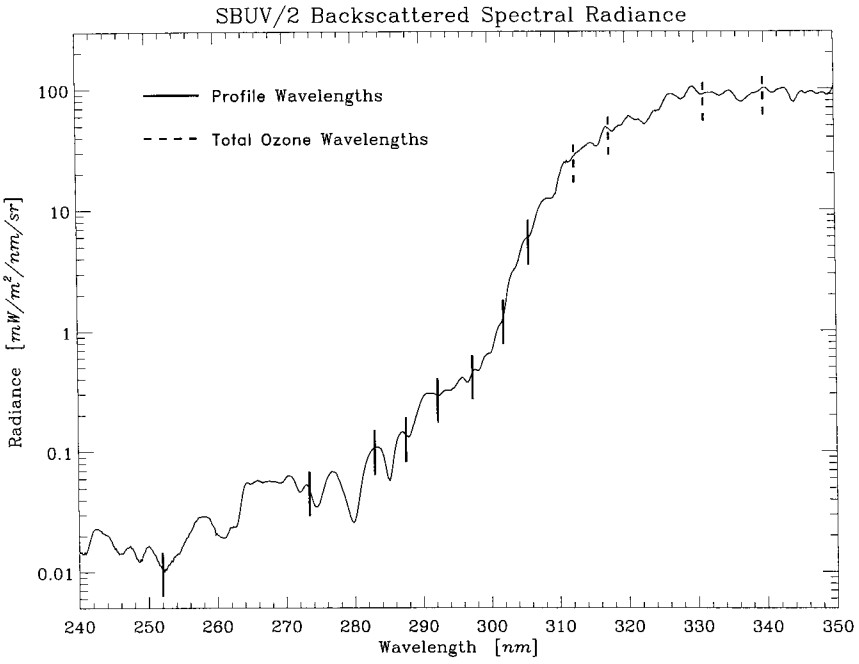

FIG. 1. Typical SBUV/2 earth radiance spectrum at a solar zenith angle of 40° over the wavelength range used for discrete ozone measurements. Wavelengths used for profile ozone derivation are indicated by solid vertical lines, and wavelengths used to calculate total ozone are shown by dashed lines.

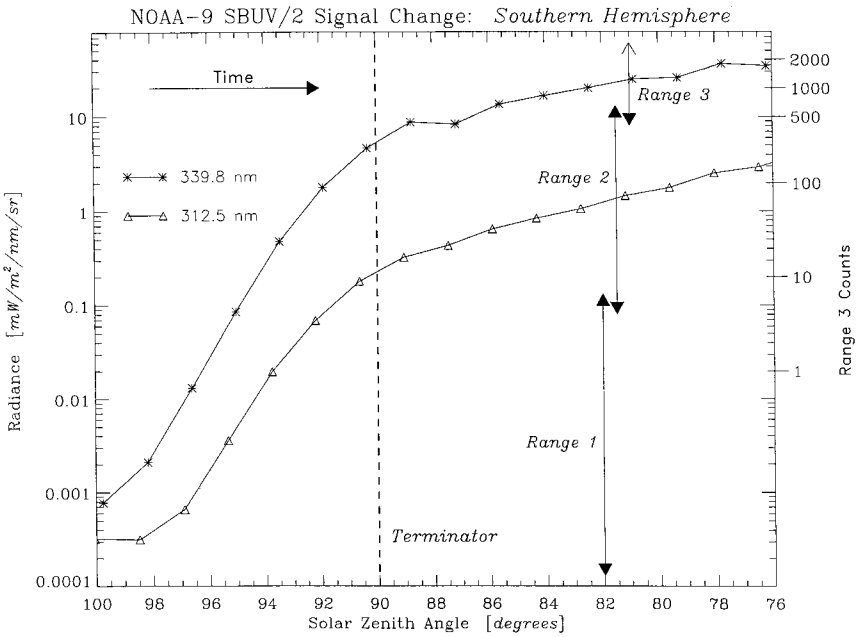

FIG. 2. Typical signal strength changes at 312.5 nm triangles and 339.8 nm (asterisks) observed at the southern terminator for *NOAA-9* SBUV/2 in Apr 1985. Each sample at a given wavelength, shown by symbols, is separated by 32 s.

tribution of samples between gain ranges. Because all output ranges are available simultaneously in the data record, carefully chosen inflight data can be used to monitor the effective PMT gain. When the input signal for range 2 or range 3 is approximately 400–800 counts, the reading from the next lower (more sensitive) gain range is also valid. The lower limit for range 3 counts is chosen to limit nonlinearity effects. For range 3 signals between 600–800 counts, the range 2 signal may overflow the 16-bit counter. Laboratory tests have established that a signal level of approximately 80 000 counts represents the saturation limit for an SBUV/2 PMT, so that range 2 overflow data up to approximately 15 000 counts can be used for analysis. The ratio of counts between the more sensitive range n_1 and the less sensitive range n_2 is called the interrange ratio (IRR_{n1n2}). The ratio between ranges 1 and 2 (IRR_{12}) is an electronic amplification only and is observed to be stable at the 0.1% level. However, the ratio between range 2 and range 3 data (IRR_{23}) provides a valuable diagnostic tool for understanding SBUV/2 instrument behavior. In particular, IRR_{23} is used to evaluate temporal changes in PMT gain and spectral changes in the semitransparent photocathode.

In its nominal midafternoon sun-synchronous orbit, an SBUV/2 instrument emerges from darkness in the Southern Hemisphere. The average PMT current increases extremely rapidly during this terminator crossing. The largest signal level changes are observed at the longest wavelengths (312.5–339.8 nm), from which total ozone is derived. Figure 2 shows the change in signal levels at the terminator crossing for a single orbit of *NOAA-9* data in April 1985. As the solar zenith angle changes from $\chi = 100°$ to $\chi = 86°$ over approximately 4 min, the SBUV/2 instrument begins to view a sunlit scene, and the signal at 339.8 nm increases by a factor of 10 000, while the signal at 312.5 nm increases by a factor of 2000. Further signal increases at lower SZA (i.e., lower latitudes) are proportional to $\cos\chi$. The overlap region in which range 2 and range 3 signals are both valid, indicated by the vertical arrows in Fig. 2, shows that IRR_{23} values can be calculated for each total ozone wavelength only in a limited range of SZA. A signal decrease of similar magnitude is observed at the northern terminator when the spacecraft moves from sunlight into darkness. Both Northern and Southern Hemispheres data can be examined as a function of solar zenith angle to examine the stability of the instrument response.

The rapid changes in input signal observed at the terminator crossings have long been recognized as a potential problem for BUV instruments. Prelaunch tests for *NOAA-9* SBUV/2 suggested that the PMT response did not stabilize until the mean tube current exceeded a minimum threshold but were unable to fully quantify this effect. Proposed physical models for PMT hysteresis suggest that the oxidized surfaces of the last stage dynode and anode, which have high resistivity, can trap the electrons or electron holes from the electron bombardment (Cantarell and Almodovar 1963; Yamashita 1978), changing the surface potential and emission and thus changing the PMT gain. The relaxation time for this process is relatively long because of the increased time required to disperse the trapped charges. Because these models predict that PMT hysteresis depends on

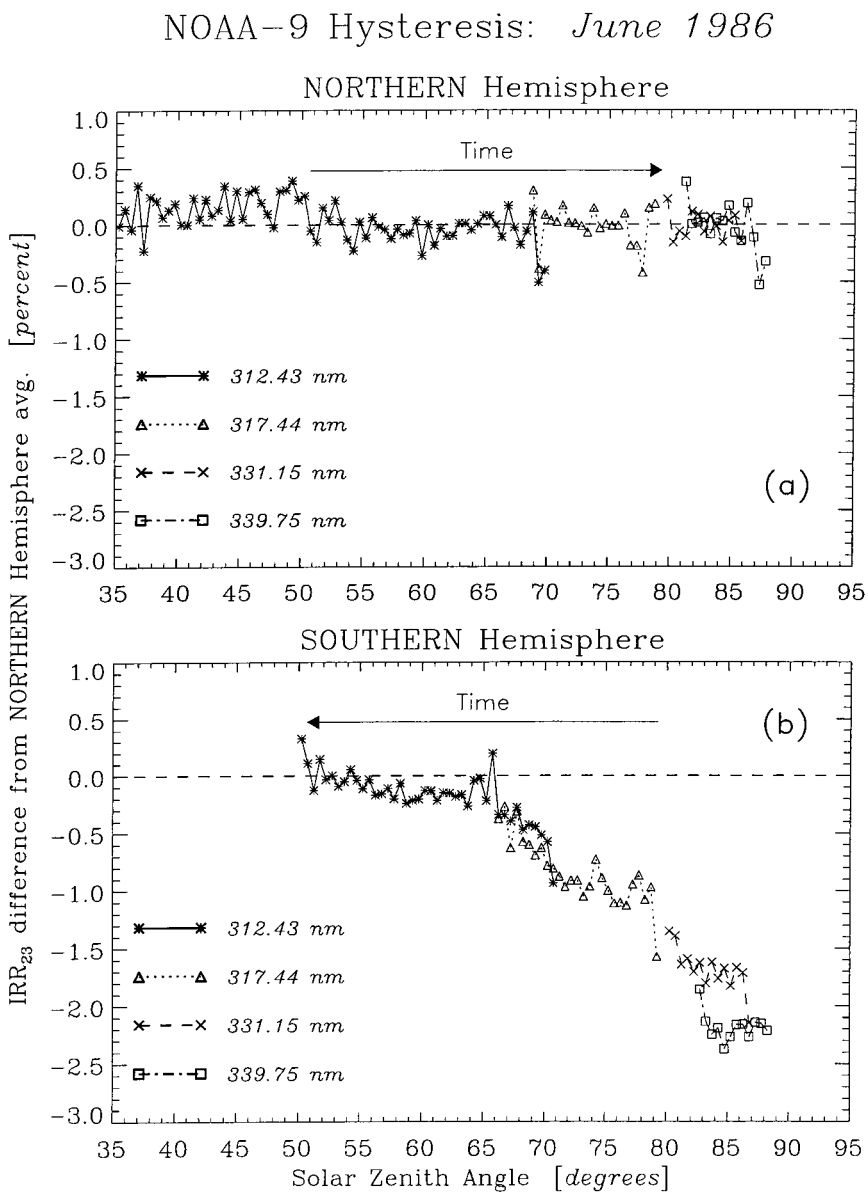

FIG. 3. The *NOAA-9* interrange ratio IRR_{23} solar zenith angle dependence during June 1986. The arrow indicates the direction of increasing time in the spacecraft orbit. All data were averaged into $\Delta\chi = 0.5^\circ$ bins for clarity. The IRR_{23} values are derived from earth view radiance measurements at wavelengths used for total ozone calculations: 312.4 nm (asterisks), 317.4 nm (triangles), 331.2 nm (crosses), 339.8 nm (squares). The average of the Northern Hemisphere data for all SZA at each wavelength was used to normalize the IRR_{23} values in both hemispheres. Panel (a) shows Northern Hemisphere data, and panel (b) shows Southern Hemisphere data.

the shape of the dynode and oxide surface layer, theoretical modeling of the impact on measurements is very difficult. It is also difficult to characterize this type of instrument response at the 1% level in the laboratory. The radiance source requirements are stringent: vary intensity by four orders of magnitude in 5 min to a 1% level of accuracy at UV wavelengths (250–340 nm), with a diffuse output to fill the $11.3^\circ \times 11.3^\circ$ SBUV/2 field of view. Such capabilities were not available in the early 1980s, when the *NOAA-9* SBUV/2 instrument was built and tested. Thus, evaluation of the inflight data becomes a key part of the overall characterization process for the SBUV/2 instrument.

3. Hysteresis effect observed for *NOAA-9* SBUV/2

Figure 3 shows the behavior of the *NOAA-9* IRR_{23} data at the total ozone wavelengths for June 1986. For each wavelength, all available data (600–3000 points) were averaged in 0.5° solar zenith angle bins for clarity.

The range of SZA for which IRR_{23} can be determined varies from approximately 83°–88° for 339.8 nm to 30°–70° for 312.5 nm due to differences in signal level at each wavelength. SZA ranges for consecutive wavelengths typically overlap. Because the absolute value of IRR_{23} is wavelength dependent, data shown here for each wavelength in both hemispheres have been normalized to the average of the Northern Hemisphere values to illustrate the relative response as a function of solar zenith angle. This step also allows an assessment of the wavelength dependence of any hysteresis effect. Theoretical models of PMT hysteresis (Yamashita 1978) suggest that it is caused by surface potential and secondary electron emission rate changes in oxide surface layers on the last dynode and anode. The SBUV/2 instrument accumulates surface charges due to photoelectron current at all wavelengths during each scan and amplifies photoelectron current caused by incoming photons using the same preconditioned surfaces. We thus expect the hysteresis effect to be wavelength independent.

Figure 3a shows a very stable IRR_{23} value with increasing SZA in the Northern Hemisphere, corresponding to decreasing signal along the orbital track. The uncertainty in this result is approximately 0.2%–0.3%. In the Southern Hemisphere, where decreasing SZA corresponds to increasing signal levels with time, a different result is found. The absolute IRR_{23} values observed are equivalent to Northern Hemisphere values at $\chi = 50°$ (Fig. 3b). However, for $\chi > 65°$, Southern Hemisphere IRR_{23} values tend to be lower than Northern Hemisphere values at the same SZA. The behavior of $IRR_{23}(\chi)$ is very consistent in regions where two wavelengths overlap, confirming the prediction that a hysteresis effect should be wavelength independent. The maximum effect is $\Delta IRR_{23} \approx -2\%$ at 339.8 nm, where valid samples are obtained at $\chi = 85°$–90°. We believe that this hysteresis effect observed in the Southern Hemisphere represents a true reduced PMT gain, which occurs because the PMT is not fully conditioned due to the rapid increase in signal. This results in lower range 2 data values relative to those recorded in range 3 for the same measurement. Examination of data for additional months shows the magnitude of the hysteresis effect to be approximately linear with SZA as the spacecraft emerges from darkness, with measurable changes disappearing by $\chi = 65°$ as the average current through the PMT during each scan reaches a threshold level. The end of the hysteresis effect is observed after approximately 8 min of sunlit data. Spacecraft telemetry for the SBUV/2 instrument only provides PMT current values every 16 s, which is insufficient to accurately characterize such a rapidly changing effect. Solar zenith angle values change approximately linearly during each scan and are highly correlated with overall changes in scene radiance. We therefore use SZA as a proxy for average PMT current in our analysis. The hysteresis effect is not observed in the Northern Hemisphere for equally rapid (decreasing) signal changes because the PMT is fully conditioned after 35–40 min of measurements during the daylight portion of the spacecraft orbit. As noted previously, there is no comparable effect between range 1 and range 2 data because both ranges are read from the last dynode of the PMT and differ only by an electronic amplification factor.

The orbit of the *NOAA-9* spacecraft drifted significantly during its operational lifetime, moving from afternoon equator-crossing times during 1985–90 to morning equator-crossing times during 1991–97. In this later period, *NOAA-9* emerged from the dark in the Northern Hemisphere. Thus, we would expect IRR_{23} data from the later part of the *NOAA-9* record to show a reversal of the hysteresis effect, with SZA-dependent IRR_{23} changes observed in the Northern Hemisphere and constant IRR_{23} values in the Southern Hemisphere. Figure 4 plots the earth view IRR_{23} data for December 1996. The format is the same as Fig. 3 except that Southern Hemisphere IRR_{23} data at each wavelength are averaged over all SZA for use as normalization values. As expected, a hysteresis effect is observed in Northern Hemisphere IRR_{23} data in 1996 (Fig. 4a), with a maximum impact of about 1.5%. Southern Hemisphere data taken at the end of the orbit show no hysteresis at high SZA (Fig. 4b).

Analysis of the entire *NOAA-9* data record suggests that the impact of the hysteresis effect on the radiance data is not constant with time. Figure 5 shows the relative magnitude of the hysteresis effect as a function of time. For each day, interrange ratio data taken at $\chi > 65°$ in the hemisphere where the spacecraft emerged from darkness were averaged together, and the difference from the average IRR_{23} value in the opposite hemisphere was calculated. The corresponding average SZA was also calculated. Using these average values, we forced the hysteresis effect to be zero at $\chi = 65°$ and extrapolated a linear SZA dependence to $\chi = 90°$. The symbols in Fig. 5 represent these maximum hysteresis effect values. The solid line is a time-dependent spline fit to the daily samples. The seasonal variations observed during 1989–93 are induced by the drifting orbit of the *NOAA-9* spacecraft. Figure 6 shows a schematic view of the hysteresis effect as it impacts the *NOAA-9* PMT gain at 339.8 nm for two different types of orbits. In a normal midafternoon orbit (Fig. 6a), the signal level (thin line) increases rapidly upon emerging from darkness. The PMT gain is reduced initially (dashed line), then reaches its nominal level by approximately $\chi = 65°$ and stays at that level throughout the orbit. When *NOAA-9* drifted into a late afternoon orbit (Fig. 6b), solar zenith angles were very high throughout the entire orbit, thus greatly reducing observed signal levels. In this situation, the PMT is never fully conditioned because average current levels remain low, and thus the gain is reduced at all times. The variation in IRR_{23} in

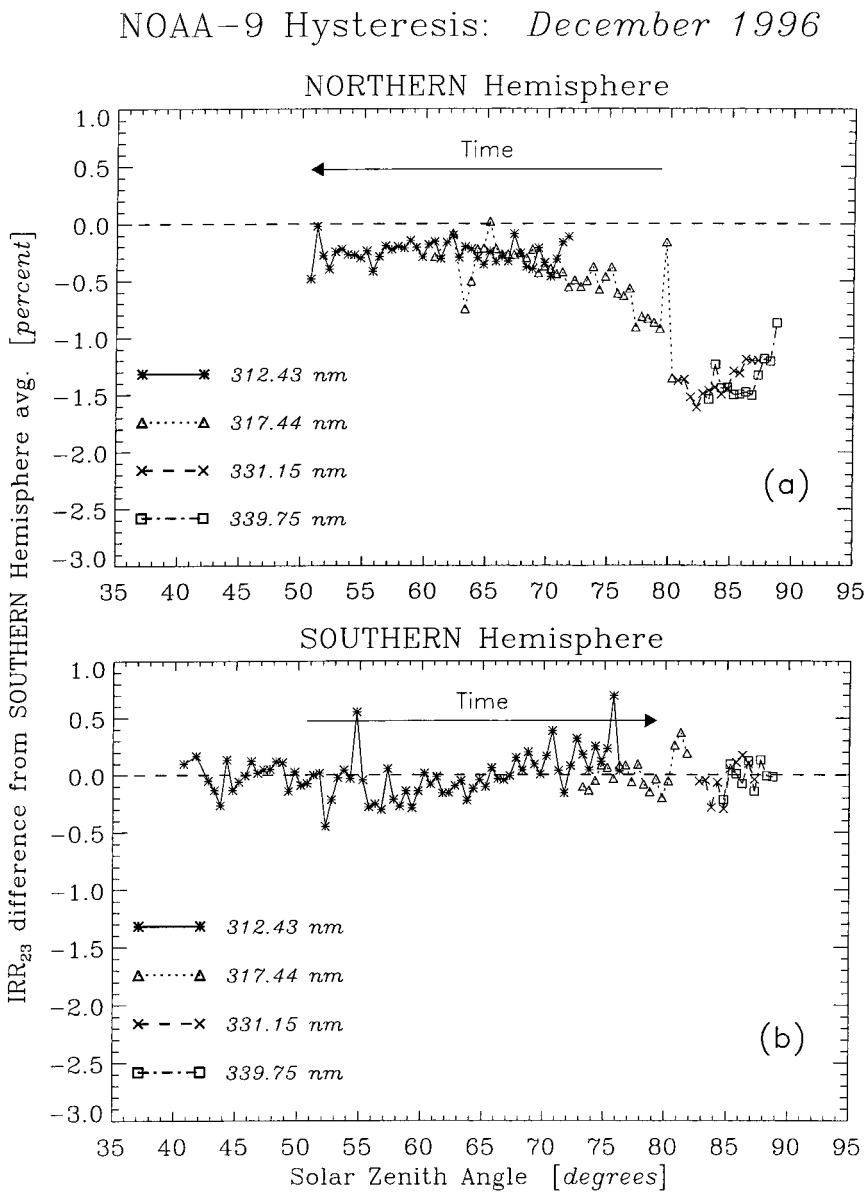

FIG. 4. The *NOAA-9* interrange ratio IRR_{23} solar zenith angle dependence during Dec 1996. The format is the same as Fig. 3. The average of the Southern Hemisphere data at each wavelength was used for normalization. (a) Northern Hemisphere data; (b) Southern Hemisphere data.

the emerging hemisphere between $\chi = 65°$ and $\chi = 90°$ is smaller, and so the *relative* hysteresis effect required to correct high SZA data is also smaller. There is an asymmetry at the 0.5% level in Fig. 5 between results derived when *NOAA-9* was in an afternoon orbit (1985–88) and results from morning orbit conditions (1994–97). This difference may be related to the fact that the afternoon orbit data affected by hysteresis were taken in the high-latitude Southern Hemisphere, where average surface reflectivity is relatively high. *NOAA-9* data taken during 1994–97 emerged from darkness in the Northern Hemisphere, where typical UV surface reflectivities are lower.

4. Operational correction for hysteresis effect

We used the smoothed curve shown in Fig. 5 to derive a relative correction for the *NOAA-9* hysteresis effect as a function of solar zenith angle and time. The correction is applied only in the hemisphere where the spacecraft emerges from darkness and only for data with SZA >65°. The operational function is given by

$$\text{counts}_{\text{range I}}(\text{true}) = \frac{\text{counts}_{\text{range I}}(\text{observed})}{1 + \left[\left(\frac{\chi - 65°}{25°}\right) A(t)\right]} \qquad (1)$$

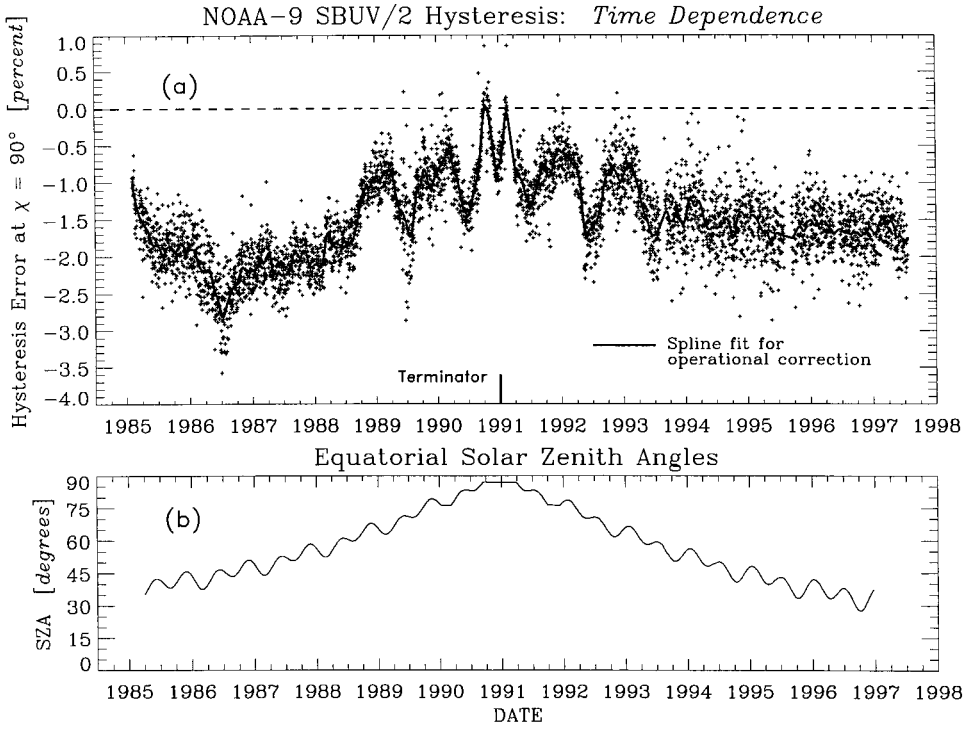

FIG. 5. (a) Time dependence of the *NOAA-9* hysteresis effect. Individual samples represent the maximum hysteresis effect at $\chi = 90°$ for each date, derived by calculating the average difference in IRR_{23} data and using a linear SZA dependence to extrapolate to $\chi = 90°$. The solid line is a smoothing spline fit to the daily values. (b) Weekly average solar zenith angle values at the equator observed by *NOAA-9*.

where $I = 1, 2$ and $\chi = [65°, 90°]$. The time-dependent magnitude $A(t)$ is taken from the spline fit in Fig. 5.

The hysteresis correction given by (1) is important in calculating the interrange ratio time dependence $IRR_{23}(t)$, which is used in ozone processing to correct for time-dependent changes in PMT gain. The $IRR_{23}(t)$ curve shown in Fig. 3a of Ahmad et al. (1994) was derived from a global average of 331.2-nm data, which included Southern Hemisphere data affected by hysteresis. This led to errors of up to 1% in daily average values and caused exaggerated short-term fluctuations during near-terminator periods. We revised the determination of $IRR_{23}(t)$ to use data measured at 312.5 nm, which is less susceptible to hysteresis errors, and also chose only samples obtained in the ''trailing'' hemisphere (Northern Hemisphere during 1985–90, Southern Hemisphere during 1991–97). The new $IRR_{23}(t)$ function accurately represents the actual PMT gain during near terminator conditions.

The impact of the hysteresis correction on total ozone values derived from *NOAA-9* measurements is dependent on the solar zenith angle and absolute ozone value of each observation, since both quantities affect the magnitude of the raw signal and thus the choice of valid gain range for each sample. The NOAA ozone processing system converts all data to equivalent range 2 signals for processing using the interrange ratio values IRR_{23} and IRR_{12} as necessary. Therefore, total ozone calculations, which use the ratio of wavelength pairs, will be impacted by the hysteresis correction when one wavelength is measured in range 3 and the other wavelength is measured in range 2. The ''best'' total ozone value reported from V6 algorithm processing is a weighted combination of ozone pairs based on measurement conditions (Herman et al. 1991). The actual impact of the hysteresis correction on the total ozone product is therefore rather complex. *NOAA-9* total ozone changes for October 1986 due to the implementation of the hysteresis correction are shown in Fig. 7, using eight consecutive days of data to provide full global coverage. Changes are shown in Dobson units (DU), where 1 DU $= 1$ m atm cm^{-1}. At this time of year, the observing geometry of *NOAA-9* was such that no hysteresis corrections were made northward of approximately 50°S latitude. In the south polar region, typical ozone changes due to the use of (1) are $\Delta\Omega \leq 4$ DU, corresponding to 1.0%–1.5% of the total column ozone abundance. Maximum hysteresis correction values of 10–12 DU are observed at approximately 80°S, which corresponds to a total ozone change of 4%–5% at this latitude and season. *NOAA-9* data are not available beyond about 81° latitude because of the inclination of the sun-synchronous orbit. The hysteresis correction was applied to all *NOAA-9* total ozone data as part of a series of improvements for trend analysis (DeLand et al. 2000).

NOAA-9 SBUV/2 measurements made at the eight

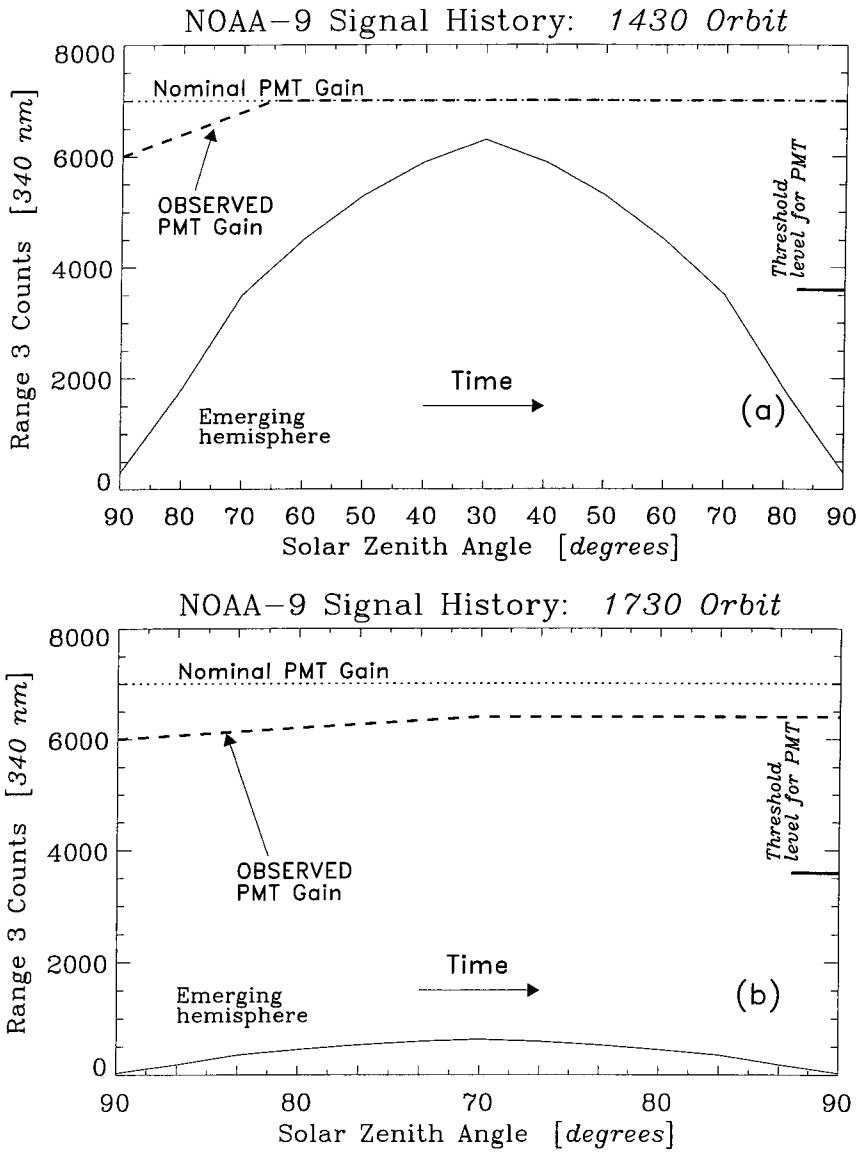

FIG. 6. Schematic diagram of hysteresis effect as observed in *NOAA-9* SBUV/2 PMT gain. (a) The thin line represents range 3 counts at 339.8 nm, plotted as a function of solar zenith angle, for the daylight portion of a typical orbit with a 1430 equator-crossing time. The horizontal dotted line illustrates the nominal PMT gain, that is, constant during the orbit. The dashed line shows the observed PMT gain, with lower values at high SZA in the emergent hemisphere. (b) Signal history and PMT gain behavior for a 1730 equator-crossing orbit. Note the difference in the solar zenith angle range during the orbit.

shortest wavelengths (252.0–305.8 nm) are used in the derivation of profile ozone. Data measured at these wavelengths typically have valid signals only in gain range 1 or range 2, and thus the observed radiance values at high solar zenith angles are impacted by the hysteresis effect. The sensitivity of the ozone profile to a constant radiance error varies significantly with altitude, as shown by Fleig et al. (1990). The maximum profile sensitivity is observed in the upper stratosphere, where a −1% error in radiance leads to a +1.9% error in ozone at 1 hPa. Thus, the maximum hysteresis correction of 2.0%–2.5% during 1986 shown in Fig. 5 represents a potential change in ozone of 4%–5% at 1 hPa. The hysteresis correction given by (1) was applied to data at all wavelengths during the recent reprocessing of *NOAA-9* ozone data (Flynn et al. 2000).

5. Other SBUV-type instruments

The SBUV/2 instruments on the *NOAA-11* and *NOAA-14* spacecraft (launched in September 1988 and December 1994, respectively) are almost identical me-

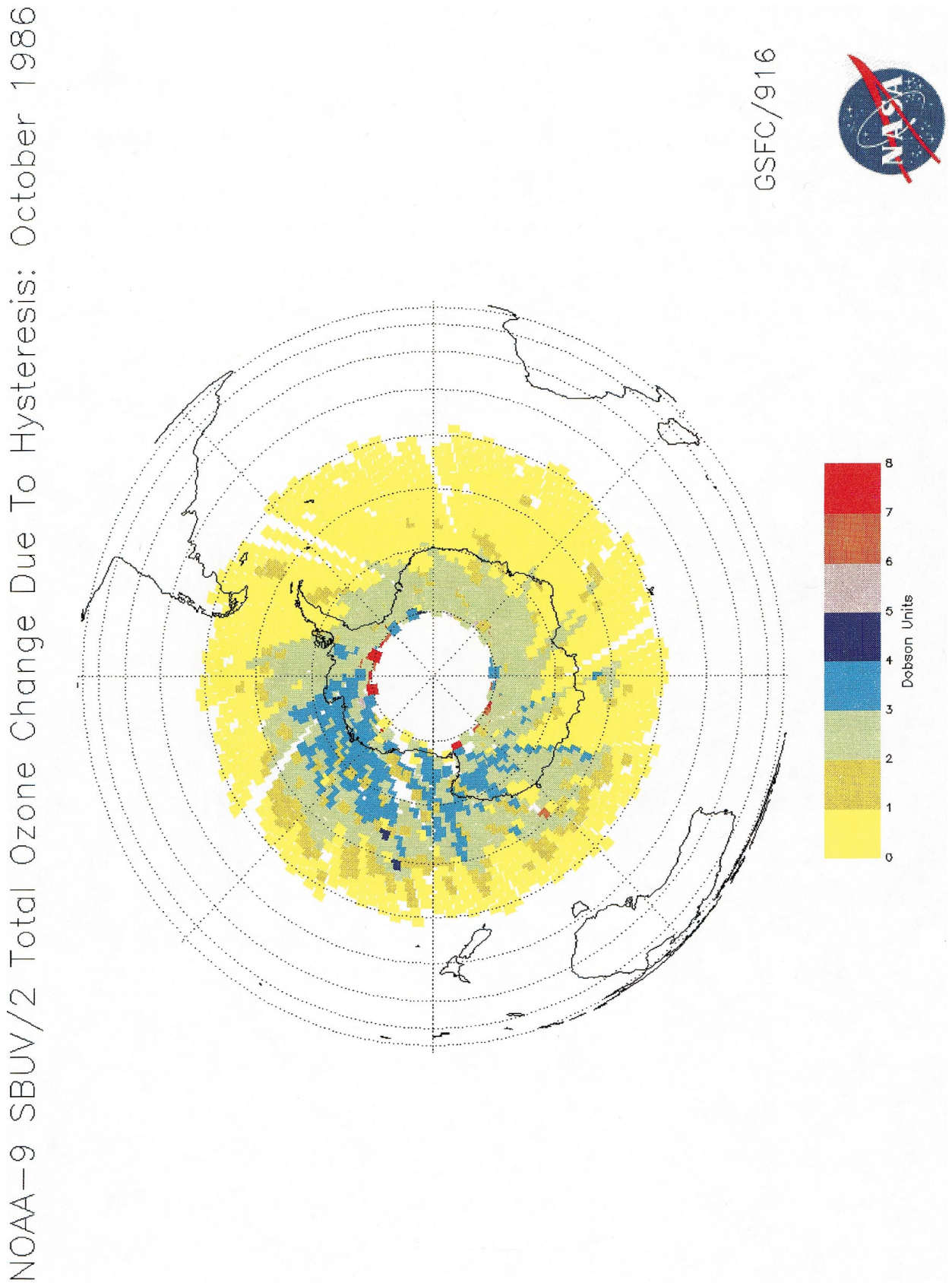

FIG. 7. Changes in *NOAA-9* SBUV/2 total ozone for Oct 1986 due to implementation of the hysteresis correction derived in section 4. Data for eight consecutive days were combined to give global coverage. All changes are given in Dobson units.

chanically to the *NOAA-9* SBUV/2 instrument and were also launched into afternoon orbits. However, after the PMT response problems were identified during *NOAA-9* prelaunch testing, a different manufacturer was selected for the PMTs used on *NOAA-11* and *NOAA-14* SBUV/2. These instruments show a greatly reduced sensitivity to hysteresis problems. An analysis of the inflight interrange ratio IRR_{23} data for *NOAA-11* finds no apparent hysteresis effect exceeding approximately 0.3%, which is the noise limit of this technique. Analysis of *NOAA-14* SBUV/2 IRR_{23} data shows no hysteresis effect in the Southern Hemisphere. There is a suggestion of hysteresis-type IRR_{23} changes up to $+0.5\%$ in the Northern Hemisphere. While this is in the opposite direction of the *NOAA-9* hysteresis effect, our understanding of PMT hysteresis at the 0.5% level does not rule out such a result. We have not implemented a hysteresis correction for *NOAA-14* SBUV/2 data at this time but plan further studies of these data and their implications.

The *Nimbus-7* SBUV and TOMS (Total Ozone Mapping Spectrometer) instruments are very similar in design and operation to the SBUV/2 series, and measurements from these instruments have also been evaluated for hysteresis effects. Radiance errors of up to 8%–10% at high solar zenith angles have been identified in *Nimbus-7* SBUV data, and Southern Hemisphere measurements taken at $\chi > 80°$ are currently not recommended for scientific use (Bhartia et al. 1995). The *Nimbus-7* TOMS data also show evidence of a hysteresis effect in the Southern Hemisphere (Wellemeyer et al. 1996). However, because this effect is wavelength independent and impacts all gain ranges, the use of wavelength pairs in the total ozone algorithm removes any hysteresis effect from the ozone product. The *Nimbus-7* SBUV instrument used a different electronic design than the SBUV/2 instruments, so that an alternative method of characterizing hysteresis errors for algorithm correction will be required. It should be noted that the stable, near-noon orbit of the *Nimbus-7* satellite leads to a repeatable pattern in Southern Hemisphere latitude for the occurrence of high SZA. Thus, the hysteresis effect in ozone for *Nimbus-7* SBUV may have an annual cycle, with modifications due to seasonal variations in ozone abundance.

6. Conclusions

Backscattered ultraviolet measurements made by polar-orbiting instruments experience a rapid change in signal level as the spacecraft emerges from darkness, which may exceed the time response of the photomultiplier tube. For *NOAA-9* SBUV/2, the lag in time response of the photomultiplier tube in such situations (''hysteresis'') leads to radiance errors as large as -3%. This effect impacts both total ozone and profile ozone values. We have characterized this effect as a function of solar zenith angle and time and implemented a correction term for ozone processing. Corresponding total ozone changes are typically 4 DU or less (1.0%–1.5%) at $\chi > 65°$, but can reach 10–12 DU (4%–5%) in some cases. Profile ozone changes will vary with altitude, reaching a maximum of 4%–5% at 1 hPa. We expect the use of this correction to significantly improve the agreement between *NOAA-9* total ozone and other datasets at high latitude. Reprocessed *NOAA-9* ozone data, which include the hysteresis correction, are available from the NOAA anonymous FTP site at orbit-net.nesdis.noaa.gov/pub/crad2/.

Acknowledgments. M. T. DeLand, R. P. Cebula, L.-K. Huang, and S. L. Taylor were supported by NASA contract NAS5-31755.

REFERENCES

Ahmad, Z., and Coauthors, 1994: Accuracy of total ozone retrieval from NOAA SBUV/2 measurements: Impact of instrument performance. *J. Geophys. Res.,* **99,** 22 975–22 984.

Bhartia, P. K., S. Taylor, R. D. McPeters, and C. Wellemeyer, 1995: Application of the Langley plot method to the calibration of the solar backscattered ultraviolet instrument on the Nimbus 7 satellite. *J. Geophys. Res.,* **100,** 2997–3004.

Cantarell, I., and I. Almodovar, 1963: Fatigue in photomultiplier tubes—An effect of the Malter type. *Nucl. Instrum. Methods,* **24,** 353–357.

DeLand, M. T., R. P. Cebula, S. L. Taylor, L. K. Huang, R. S. Stolarski, and R. D. McPeters, 2000: Calibration of NOAA-9 and NOAA-11 SBUV/2 total ozone data for trend analysis. *Proc. Quadrennial Ozone Symp.,* Sapporo, Japan, Int. Ozone Comm., 53–54.

Fleig, A. J., R. D. McPeters, P. K. Bhartia, B. M. Schlesinger, R. P. Cebula, K. F. Klenk, S. L. Taylor, and D. F. Heath, 1990: Nimbus 7 Solar Backscatter Ultraviolet (SBUV) Ozone Products User's Guide. NASA Ref. Pub. RP-1234, 128 pp.

Flynn, L. E., S. Kondragunta, K. Horvath, and E. Beach, 2000: Internal validation of SBUV/2 ozone vertical profile data sets. *Proc. Quadrennial Ozone Symp.,* Sapporo, Japan, Int. Ozone Comm., 75–76.

Frederick, J. E., R. P. Cebula, and D. F. Heath, 1986: Instrument characterization for the detection of long-term changes in stratospheric ozone: An analysis of the SBUV/2 radiometer. *J. Atmos. Oceanic Technol.,* **3,** 472–480.

Heath, D. F., C. L. Mateer, and A. J. Krueger, 1973: The Nimbus-4 backscatter ultraviolet atmospheric ozone experiment—Two years' operation. *Pure Appl. Geophys.,* **106–108,** 1238–1253.

——, A. J. Krueger, H. A. Roeder, and B. D. Henderson, 1975: The Solar Backscatter Ultraviolet and Total Ozone Mapping Spectrometer (SBUV/TOMS) for Nimbus G. *Opt. Eng.,* **14,** 323–331.

Herman, J. R., R. Hudson, R. D. McPeters, R. S. Stolarski, Z. Ahmad, X. Y. Gu, S. Taylor, and C. Wellemeyer, 1991: A new self-calibration method applied to TOMS/SBUV backscattered ultraviolet data to determine long-term global ozone change. *J. Geophys. Res.,* **96,** 7531–7545.

Hilsenrath, E., R. P. Cebula, M. T. DeLand, K. Laamann, S. Taylor, C. Wellemeyer, and P. K. Bhartia, 1995a: Calibration of the NOAA 11 SBUV/2 ozone data set from 1989 to 1993 using in-flight calibration data and SSBUV. *J. Geophys. Res.,* **100,** 1351–1366.

——, M. T. DeLand, and R. P. Cebula, 1995b: Initial solar irradiance measurements from the NOAA-14 SBUV/2 instrument. *EOS, Trans. Amer. Geophys. Union,* **76** (Suppl.), p. 239.

Lienesch, J. H., W. G. Planet, M. T. DeLand, K. Laamann, R. P. Cebula, E. Hilsenrath, and K. Horvath, 1996: Validation of NOAA-9 SBUV/2 total ozone measurements during the 1994 Antarctic ozone hole. *Geophys. Res. Lett.,* **23,** 2593–2596.

Planet, W. G., and Coauthors, 1994: Northern Hemisphere total ozone values from 1989–1993 determined with the NOAA-11 Solar Backscatter Ultraviolet instrument. *Geophys. Res. Lett.,* **21,** 205–208.

Singer, S. F., and R. C. Wentworth, 1957: A method for the determination of the vertical ozone distribution from a satellite. *J. Geophys. Res.,* **62,** 299–308.

Stolarski, R. S., G. J. Labow, and R. D. McPeters, 1997: Springtime Antarctic total ozone measurements in the early 1970s from the BUV instrument on Nimbus 4. *Geophys. Res. Lett.,* **24,** 591–594.

Wellemeyer, C. G., S. L. Taylor, G. Jaross, M. T. DeLand, C. J. Seftor, G. Labow, T. J. Swissler, and R. P. Cebula, 1996: Final Report on Nimbus-7 TOMS Version 7 Calibration. NASA Tech. Rep. CR-4717, 54 pp.

Yamashita, M., 1978: Mechanism of the hysteresis effect in rate-dependent photomultiplier gain variations. *Rev. Sci. Instrum.,* **49,** 1336–1342.